NeuroImage: Clinical 13 (2017) 70–81

Contents lists available at ScienceDirect

NeuroImage: Clinical

journal homepage: www.elsevier.com/locate/ynicl

Resting state functional network disruptions in a kainic acid model of temporal lobe epilepsy

Ravnoor Singh Gill[a,f], Seyed M. Mirsattari[a,b,c,d,e], L. Stan Leung[a,f,*]

[a] Graduate Program in Neuroscience, Western University, London, Ontario, Canada
[b] Clinical Neurological Sciences, Western University, London, Ontario, Canada
[c] Department of Biomedical Imaging, Western University, London, Ontario, Canada
[d] Department of Biomedical Physics, Western University, London, Ontario, Canada
[e] Department of Psychology, Western University, London, Ontario, Canada
[f] Department of Physiology & Pharmacology, Western University, London, Ontario, Canada

ARTICLE INFO

Article history:
Received 20 May 2016
Received in revised form 19 October 2016
Accepted 1 November 2016
Available online 3 November 2016

Keywords:
Temporal lobe epilepsy
Limbic system
Default mode network
Resting-state networks
Kainic acid
Functional connectivity

ABSTRACT

We studied the graph topological properties of brain networks derived from resting-state functional magnetic resonance imaging in a kainic acid induced model of temporal lobe epilepsy (TLE) in rats. Functional connectivity was determined by temporal correlation of the resting-state Blood Oxygen Level Dependent (BOLD) signals between two brain regions during 1.5% and 2% isoflurane, and analyzed as networks in epileptic and control rats. Graph theoretical analysis revealed a significant increase in functional connectivity between brain areas in epileptic than control rats, and the connected brain areas could be categorized as a limbic network and a default mode network (DMN). The limbic network includes the hippocampus, amygdala, piriform cortex, nucleus accumbens, and mediodorsal thalamus, whereas DMN involves the medial prefrontal cortex, anterior and posterior cingulate cortex, auditory and temporal association cortex, and posterior parietal cortex. The TLE model manifested a higher clustering coefficient, increased global and local efficiency, and increased small-worldness as compared to controls, despite having a similar characteristic path length. These results suggest extensive disruptions in the functional brain networks, which may be the basis of altered cognitive, emotional and psychiatric symptoms in TLE.

1. Introduction

1.1. Temporal lobe epilepsy and networks

Temporal lobe epilepsy (TLE) is a common type of focal epilepsy. It is characterized by spontaneously recurring focal dyscognitive seizures that originate from the temporal lobe, often from mesial structures such as the hippocampus and amygdala. In about one-third of the patients with TLE, it is debilitating because it is difficult to control by antiepileptic drugs (AEDs), and often associated with behavioural, cognitive and psychiatric disturbances in the interval between seizures (i.e. interictal period) or immediately after the seizures (i.e. postictal period).

The interictal behavioural and cognitive disturbances in TLE suggest that large areas of the brain are affected. A temporal lobe seizure may spread to many brain areas directly and indirectly connected to the temporal lobe, which include limbic and frontal brain structures (Bartolomei et al., 2004; Bertram et al., 1998). These findings suggest a deleterious impact of TLE on the whole brain, potentially impacting multiple brain networks (Laufs, 2012; Morgan et al., 2011; Tracy et al., 2014).

1.2. Resting state networks and graph theoretical networks

In functional magnetic resonance imaging (fMRI), the correlations between spontaneous low-frequency fluctuations of a Blood Oxygen Level Dependent (BOLD) signal provide a measure of the functional connectivity in normal and pathological condition. A prominent resting state network (RSN) in normal subjects is the default mode network (DMN) involving the medial prefrontal cortex, medial temporal lobe and cingulate cortex (Gozzi and Schwarz, 2016; Greicius et al., 2009). DMN appears to be homologous across humans, monkeys, and rodents (Lu et al., 2012; Sierakowiak et al., 2015). The DMN is most active at rest (awake with eyes closed), and persists in moderate anaesthesia (Hutchison et al., 2014; Wang et al., 2011). DMN disruptions and disconnection with other parts of the brain have been reported during the interictal state in TLE patients (Laufs et al., 2007; Liao et al., 2010).

Topological properties of a brain network can be analyzed by graph theoretical analysis (Bullmore and Sporns, 2009), by representing brain regions as nodes and structural/functional connection pathways as

* Corresponding author at: Department of Physiology and Pharmacology Medical Sciences Building, The University of Western Ontario, London N6A 5C1, Ontario, Canada.
E-mail addresses: rsing96@uwo.ca (R.S. Gill), Seyed.Mirsattari@lhsc.on.ca (S.M. Mirsattari), sleung@uwo.ca (L.S. Leung).

http://dx.doi.org/10.1016/j.nicl.2016.11.002

edges. In a graph theoretical framework, functional networks can be objectively characterized by different mathematical measures (see Rubinov and Sporns, 2010, for a non-technical review). Watts and Strogatz (1998) defined small-world networks as a class of networks with significantly more clustering than random networks, while still having a similar characteristic path length as random networks. Networks in the brain are hypothesized to optimize local processing and global integration (Meador, 2011; Stam and Reijneveld, 2007b). In TLE patients, controlling abnormal networks can play a substantial role in guiding targeted interventions and therapies (Lopes da Silva et al., 2012).

A host of studies investigating structural and functional interictal brain networks in TLE patients and control subjects, using EEG, MEG and MRI, have yielded mixed and ambiguous results (see Bernhardt et al., 2015, for review). Irreconcilable bidirectional changes in both the network connectivity and the graph theoretical measures have been reported. For instance, using fMRI data, Liao et al. (2010) reported reduced clustering coefficients and path lengths along with an increased connectivity within the medial temporal lobe and decreased connectivity within the DMN. Vaessen et al. (2012) reported reduced clustering but increased path lengths in TLE patients with cognitive decline, while Chiang and Haneef (2014a) reported increase in clustering and path lengths. Increase in clustering and path lengths in TLE patients was also found using structural MRI data (Bernhardt et al., 2011) or EEG data (Horstmann et al., 2010). Thus, while TLE patients appear to exhibit disruptions of both local segregation and global integration, the actual change remains unequivocal.

The inconsistent results on TLE patients could result from heterogeneity of the patient population. In addition, because of preexisting genetic factors and patient-selective history, it is unclear whether the disruptions of RSNs in human TLE are caused by seizure activity only. In addition, ethical concerns prevent experimental studies in humans, although these studies are necessary to elucidate the underlying mechanisms. Thus, we used an animal model of TLE in an attempt to study the RSN disruptions in human TLE.

1.2.1. Study of resting state networks in an animal model of TLE

The TLE model selected was kainic acid induced status epilepticus (SE) in rats. Systemic administration of kainic acid in rats leads to prolonged limbic seizures lasting for several hours, and with increasing severity indicated by wet-dog shakes, facial and forelimb clonus, and then rearing, falling and jumping (Dudek and Edward, 2005). Following a seizure-free latent period of 2–3 weeks, kainate-treated epileptic rats manifested spontaneous recurrent seizures throughout their lifespan (Sperk et al., 1985). The behavioural, electroencephalographic, and neuropathological features of the kainate-induced model resemble those of human TLE (Buckmaster, 2004; Dudek and Edward, 2005; Lévesque and Avoli, 2013).

The present study focuses on characterizing alterations in the resting-state networks of kainate-treated epileptic rats. This follows our original report of multiple RSNs in anaesthetized rats (Hutchison et al., 2010). To our knowledge, RSNs have not been studied in animal models of TLE. In a tetanus toxin induced rat model of neocortical focal epilepsy, Otte et al. (2012) demonstrated an increase in clustering and path length.

The objective of this study was to elucidate the changes in functional connectivity between various regions of the brain in a model of TLE in rats, by recording fMRI BOLD signals in kainate-treated epileptic rats and age-matched, saline-treated controls. We hypothesized that both the local and global functional connectivity will be significantly altered in this rodent model of TLE, as analyzed by a graph theoretical approach.

2. Materials & methods

2.1. Animals

Adult male Long-Evans rats (Charles River, St. Constance, Quebec, Canada) weighing 250–400 g were used in these experiments. Rats were housed in standard cages and subjected to 12:12 h light (7–19 h)/dark cycle. Food and water was accessible ad libitum, in a temperature regulated environment. The study was conducted in accordance with the guidelines established by the Canadian Council on Animal Care and approved by the local Animal Use Subcommittee. All experiments were conducted during the light phase (8–19 h).

2.2. Induction of spontaneous seizures using kainic acid

Kainic acid (Abcam Biochemicals, Cambridge, MA) was administered intraperitoneally (i.p.), using an incremental dose protocol modified from (Dudek and Edward, 2005), to induce SE in rats. Adult male rats were randomly allocated to either sham saline treatment ($n = 11$; initial weight 255 ± 5.8 g, mean ± standard error of the mean (SEM)) or kainic acid treatment, of which 8 rats with spontaneous seizures were used for fMRI connectivity study (initial weight: 247 ± 3.9 g, $n = 8$; not different from saline group). In the kainate group, rats were injected with an initial dose of 5 mg/kg i.p. kainic acid (diluted to 10 mg/mL with sterile saline), and monitored for behavioural seizures stages according to Racine (1972) [stage 3, forelimb clonus; stage 4, rearing with forelimb clonus; stage 5, rearing and falling with forelimb clonus]. If convulsive (>stage 3) seizure did not occur, a subsequent half dose of 2.5 mg/kg was administered at ~1 h after the initial dose. Incremental repeated doses (2.5–5.0 mg/kg) were administered to the rats until they developed stage 5 seizures or exhibited convulsive (stage 3 to 5) seizures for >3 h. Age matched controls were injected with a similar volume of sterile saline (0.1–0.2 mL i.p.) as kainic acid injected rats. Diazepam (Sandoz, Canada; 5 mg/mL) was administered (4 mg/kg i.p.) to stop the seizures after 3 h of stage 5 seizure. Sterile saline (1.5–2.5 mL, 2×) was administered subcutaneously to hydrate the rats; shortly after diazepam. Starting 2–3 weeks following seizure induction, kainate-treated rats were monitored for signs of behavioural seizure activity, for 1–2 h every other day, with at least one overnight video monitoring at 3 weeks. Only animals that showed 2 or more spontaneous seizures over a period of 2 to 3 weeks were used for scanning.

2.3. Functional magnetic resonance imaging procedures

2.3.1. Animal usage and preparation

The first scan was taken 4–5 weeks after the kainate/saline-treatment. The occasional rats that showed behavioural seizure activity on the day of the scan were excluded. General anaesthesia in rats was induced with 5% isoflurane in oxygen flowing at 1.5 L/min from a calibrated vapourizer (Harvard Apparatus, Holliston, MA). Once under anaesthesia, 2% isoflurane was delivered via a custom nose-cone (serving partially as a bite bar), and the rat was secured to a custom-built nylon stereotaxic frame with ear bars (Mirsattari et al., 2005), with the frame sitting on a cradle that was later inserted into the bore of the scanner. Respiration was spontaneous throughout the experiment, and was monitored by a pneumatic pillow (SA Instruments, Stony Brook, NY) wrapped around the rat's chest wall. The rat's body temperature was maintained at 37 °C via a feedback-controlled system, using a rectal fiber-optic probe (SA Instruments) and a water-circulated heating pad (TP500, Gaymar Industries, Orchard Park, NY). Heart rate and blood oxygen saturation level were measured using a pulse oximeter (MR-compatible; 8600 V, Nonin Medical, Plymouth, MN) positioned on the hind-paw. Physiological parameters were in the normal range (temperature: 37 ± 0.5 °C, heart rate: 250–390 beats/min, breathing rate: 60–90 breaths/min, oxygen saturation: >95%) for the entire recording/scanning session.

2.3.2. Image acquisition

A minimum of 30 min was allowed for equilibration at 2% isoflurane, during which shimming and image localization were performed. Then the rats were scanned for approximately 60 min at 4 end-tidal isoflurane concentrations in the order of 2.0%, 1.5%, 1.0%, and 0.5%

(2 × 10 min scan at each concentration), and continued until the rat exhibited any movement. Movement during the scan was monitored using the heart rate and breathing rate, and by visually inspecting the EPIs overlaid on the anatomical post-scan. Since the isoflurane ED50 for loss of righting reflex in control Long-Evans rats was 1.0% (Leung et al., 2013), scans at 1–0.5% isoflurane showed increasingly movements and were excluded from the present analysis. Only the second scan at 2% and 1.5% isoflurane were used for analysis in this report.

All experiments were accomplished using a Varian Direct Drive imaging console (Palo Alto, CA), with a Magnex 31 cm actively shielded 9.4 T horizontal bore magnet equipped with an actively shielded gradient set (12 cm ID, SR 3000 $mT \cdot m^{-1} \cdot s^{-1}$; Yarnton, UK). An optimized custom built 1.5 × 2.0 cm linear transmit-receive surface coil was positioned proximally to the anterior aspect of the rat's head for imaging (Hutchison et al., 2010). Magnetic field optimization over the volume of interest was accomplished using an automated shimming algorithm (RASTAMAP, Klassen and Menon, 2004). Thirteen coronal slices of 1-mm thickness spanning the nucleus accumbens (A ~ 2.0 mm), to the entorhinal cortex (P ~ 8.0 mm) were selected using the Paxinos and Watson (2007) atlas. A fast spin echo (FSE) anatomical [effective echo train (TE) 40 ms, reception time (TR) 5 s, echo train length (ETL) 4] was acquired with a 256 × 256 matrix and a field of view (FOV) of 25.6 × 25.6 mm^2, corresponding to an in-plane spatial resolution of 100 × 100 μm^2. Functional images were acquired using an echo planar imaging sequence (TE 15 ms, repetition time TR 1000 ms, flip angle 60°), with a 64 × 64 matrix, and a FOV of 25.6 × 25.6 mm^2, corresponding to an in-plane spatial resolution of 400 × 400 μm^2. For each fMRI run, 600 images were acquired over 10 min (1 whole brain volume every second).

2.3.3. Image preprocessing and analysis

Preprocessing was carried out using command-line tools bundled within the FSL (Jenkinson et al., 2012) and AFNI (Cox, 1996) framework. First 30 volumes (initial TRs) were removed to allow magnetization equilibrium (steady state), and all volumes were registered to the first volume in the fMRI datasets to correct for minor movements. Trilinear three-dimensional (3D) head motion correction and in-plane spatial smoothing using a 2D Gaussian filter (full-width at half-maximum, FWHMxy = 0.8 × 0.8 mm^2) was applied in tandem to each EPI data set. Functional to structural space registration was achieved using FLIRT (FSL toolbox) with affine transformation (12 DOF). An eighth-order Chebyshev (Type I bandpass, ~0.01–0.1 Hz) filter with peak-to-peak passband ripple of 0.1 dB was implemented in Matlab (Mathworks, Natick, MA) and applied to all time courses on a voxel by voxel basis over the entire EPI functional (3D + time) dataset (Hampson et al., 2002).

Standardized rat templates were not used owing to low degrees of freedom inherent in the data (13 slices) relative to high dimensionality (≥100 slices with finer resolution) of the template data. The accuracy of projection of identified brain structures onto standard templates has not been tested rigorously in rats. Instead of using standardized templates, 35 regions-of-interest (ROIs) were selected, with 33 of them targeting brain areas, and 2 of them deliberately targeting cerebrospinal fluid in the lateral ventricle, to serve as zero/null connectivity controls. The location of each ROI was identified on the anatomical structural scans, by means of its geometric relation with respect to prominent anatomical landmarks, using the Paxinos and Watson (2007) rat brain atlas (see Supplementary Fig. S1 for representative location of each ROI).

Seed regions were selected in the following medial- and extra-temporal regions in both hemispheres independently: medial frontal cortex, piriform cortex, hippocampus, mediodorsal thalamus (MDT), orbitofrontal cortex, prefrontal cortex, posterior parietal cortex, auditory/temporal association cortices, anterior/posterior cingulate cortex, nucleus accumbens and amygdala (see Table 1 for a complete list of ROIs, see Supplementary Table S1 for number of voxels per ROI). Voxel resolution prevented subdividing the hippocampus into subfields, and the entorhinal and perirhinal cortices were not included because of low signals at the ventral brain.

2.3.3.1. Network-based statistic. The extracted BOLD time courses averaged over the seed region were cross-correlated with all other ROIs to derive a connectivity map. For statistical analysis, the Pearson's correlation coefficients (r) were gaussianized using the Fisher's r-to-Z transformation, $Z = 0.5 * \ln[(1+r)/(1-r)]$. Network-based statistic (NBS, http://www.nitrc.org/projects/nbs/) approach was implemented to localize specific connected components in which the functional connectivity was significantly different between the two groups. NBS is a method to adjust for multiple comparisons in graphs – by controlling the link-based family-wise error (FWE) rate when mass-univariate hypothesis testing is performed at each connection within the graph (Zalesky et al., 2010). Briefly, most consistent connections were recognized within each group. Consequently, a t-statistic is computed for each connection (node-to-node; $t \geq 3.5$, $P < 0.05$) to construct a subset of suprathreshold links for the most consistent connections. Connected components along with the number of links/connections present in the set of suprathreshold links were thus identified. To estimate the statistical significance of each component, the null distribution of the connected component size was empirically derived using a nonparametric permutation approach (5000 permutations). Ultimately, a corrected P value for a connected component of size M found in the non-randomized data was then determined by computing the proportion of the 15,000 permutations for which the maximal connected component was significantly larger than M (Wang et al., 2013a).

2.3.3.2. Graph metrics and random network generation. The significant supra-threshold links were visualized as a graph network using the Gephi software (Bastian et al., 2009). The various graph-based metrics [weighted clustering coefficient (C_w), characteristic path length (L_w), global efficiency (E_{glob}), local efficiency (E_{loc}), and small-world characteristics (γ, λ, σ)] were computed using the brain connectivity toolbox (BCT, http://www.brain-connectivity-toolbox.net; Rubinov and Sporns, 2010). Nonparametric Wilcoxon signed rank tests and nonparametric permutation tests (Wang et al., 2013b) were conducted to test differences in each of the graph-based metrics across the two groups.

Stam et al., (2007a) and Stam and Reijneveld, (2007b) suggested that statistical comparisons should generally be performed between networks with equal (or at least similar) degree sequence. However, theoretical random networks are characterized by Gaussian degree distributions, which may be incongruous with the degree distribution of the functional brain networks. Therefore, we generated, for a single threshold ($r \geq 0.3$), 100 synthetic undirected random networks with preserved degree distribution (from the KA/saline-treated brain networks) of size 35 × 35 using BCT. Then, we averaged across all 100 generated random networks, and binarized, to obtain the mean clustering coefficient, C_{random}, and the mean path length, L_{random}, of an equivalent random network.

2.4. Histology

At the end of the experiments, all rats were euthanized by 80 mg/kg i.p. pentobarbital, and the brain was perfused with saline followed by 2% formaldehyde. Coronal sections of 40 μm thick were cut in the frozen brain by a microtome and stained with thionin (Supplementary Fig. S1). For the 8 kainate-treated rats and 7 control-treated rats used in this study, histological sections containing the ROIs used in fMRI were assessed blindly for neuronal damage on a scale of 1 to 4, with 1 representing no obvious damage, 2 representing mild damage, 3 representing obvious damage and 4 representing complete lesion of the structure.

Table 1
Regions of Interest (ROIs) selected for functional connectivity, and the corresponding labels in the Paxinos and Watson (2007) atlas.

ROI #	Acronym	Acronym	Substructures (see Paxinos and Watson, 2007, rat brain atlas)
1	Orbital frontal cortex - LH	ofc-l	Lateral orbital cortex (LO), ventral orbital cortex (VO)
2	Prelimbic cortex - LH	prl-l	Prelimbic cortex (PrL)
3	Nucleus accumbens core - LH	acbc-l	Accumbens nucleus, core (AcbC)
4	Nucleus accumbens shell - LH	acbsh-l	Accumbens nucleus, shell (AcbSh)
5	Caudate putamen - LH	cpu-l	Caudate putamen [striatum] (CPu)
6	Anterior cingulate cortex - LH	acc-l	Cingulate cortex, area 1 (Cg1), cingulate cortex, area 2 (Cg2)
7	Primary somatosensory cortex - LH	sm1-l	Primary somatosensory cortex, barrel field (S1BF)
8	Secondary somatosensory cortex - LH	sm2-l	Secondary somatosensory cortex (S2)
9	Globus pallidus - LH	gp-l	GP
10	Piriform cortex - LH	pir-l	Piriform cortex (Pir)
11	Retrosplenial cortex - LH	rsp-l	Retrosplenial dysgranular cortex (RSD), retrosplenial granular cortex, c region (RSGc)
12	Mediodorsal thalamic nuclei - LH	mdt-l	Mediodorsal thalamic nucleus, lateral part (MDL), mediodorsal thalamic nucleus, medial part (MDM)
13	Amygdala - LH	amy-l	Basolateral amygdaloid nucleus, anterior part (BLA), basolateral amygdaloid nucleus, posterior part (BLP)
14	Hippocampus - LH	hc-l	Field CA1 of the hippocampus (CA1), field CA3 of the hippocampus (CA3)
15	Auditory/temporal association cortex - LH	aud-l	Primary auditory cortex (Au1), secondary auditory cortex, dorsal area (AuD), secondary auditory cortex, ventral area (AuV), temporal association cortex (TeA)
16	Posterior parietal cortex - LH	ppc-l	Parietal cortex, posterior area, dorsal part (PtPD), parietal cortex, posterior area, dorsal part (PtPR)
17	Medial septum	ms	Medial septum (MS)
18	Orbital frontal cortex - RH	ofc-r	LO, VO
19	Prelimbic cortex - RH	prl-r	PrL
20	Nucleus accumbens core - RH	acbc-r	AcbC
21	Nucleus accumbens shell - RH	acbsh-r	AcbSh
22	Caudate putamen - RH	cpu-r	CP
23	Anterior cingulate cortex - RH	acc-r	Cg1, Cg2
24	Primary somatosensory cortex - RH	sm1-r	S1BF
25	Secondary somatosensory cortex - RH	sm2-r	S2
26	Globus pallidus - RH	gp-r	Globus pallidus (GP)
27	Piriform cortex - RH	pir-r	Pir
28	Retrosplenial cortex - RH	rsp-r	RSD, RSGc
29	Mediodorsal thalamic nuclei - RH	mdt-r	MDL, MDM
30	Amygdala - RH	amy-r	BLA, BLP
31	Hippocampus - RH	hc-r	CA1, CA3
32	Auditory/temporal association cortex - RH	aud-r	Au1, AuD, AuV, TeA
33	Posterior parietal cortex - RH	ppc-r	PtPD, PtPR
34	Cerebrospinal fluid (ventricles) - 1	csf1	Choroid plexus (chp, cerebrospinal fluid)
35	Cerebrospinal fluid (ventricles) - 2	csf2	Choroid plexus (chp, cerebrospinal fluid)

3. Results

3.1. Functional connectivity of kainate and control rats

Data were obtained from 8 kainate-treated and 11 control rats, at 2.0% followed by 1.5% isoflurane concentrations. Functional connectivity between a pair of seed regions was computed from their respective time series (570 s) in each subject, and averaged for each group ($n_{kainate} = 7$, $n_{saline} = 7$ for 2.0% isoflurane; and $n_{kainate} = 8$, $n_{saline} = 7$ for 1.5% isoflurane). The mean correlation across pairs of the 35 seed regions (33 brain regions and 2 ventricles with expected zero connectivity) is shown as a 35×35 matrix at the top of Figs. 1 and 2. The correlations were arbitrarily thresholded to generate sparse matrices (bottom of Figs. 1 and 2). The ROIs that were significantly different between kainate and control groups were chosen as nodes, and an edge was defined to be a statistically significant connection between two nodes; this connection was undirected and implied no causality. The sparse/binary matrices were used to derive graph networks, with each above-threshold ROI serving as a node, a statistically significant connection between two nodes considered an edge in an undirected (no causality) network. Graph theory measures, such as weighted clustering coefficient (C_w), characteristic path length (L_w), global efficiency (E_{glob}), local efficiency (E_{loc}), and small-world characteristics (γ, λ, σ) were then estimated.

3.1.1. Differences in connectivity at 1.5% isoflurane

Network based-statistic (NBS) was used to reveal nodes that were significantly well-represented (intra-group). There were 33 nodes and 420 edges ($P \leq 0.001$) in the kainate group, as compared to 69 edges and 22 nodes ($P \leq 0.007$) in the control group. NBS was further used to determine the network components that were significantly different between the two groups (inter-group). The analysis revealed a single sub-network comprising of 23 nodes and 78 edges (among a total possible combination of $0.5 * {}^{33}C_2 = 264$ edges) that was significantly higher in the kainate than the control group (Fig. 3A, $P \leq 0.003$). No nodes and edges corresponded to a reduced connectivity in the kainate group compared to the control group (Fig. 4). A significant number of nodes were localized in the medial temporal lobe regions, along with other subcortical regions like the nucleus accumbens and the MDT (Fig. 4). Nodes were also identified in components of the DMN (anterior and posterior cingulate cortex and auditory/temporal association cortex) and the somatosensory system (primary/secondary somatosensory cortex). The specific ROI connections are detailed in Table 2.

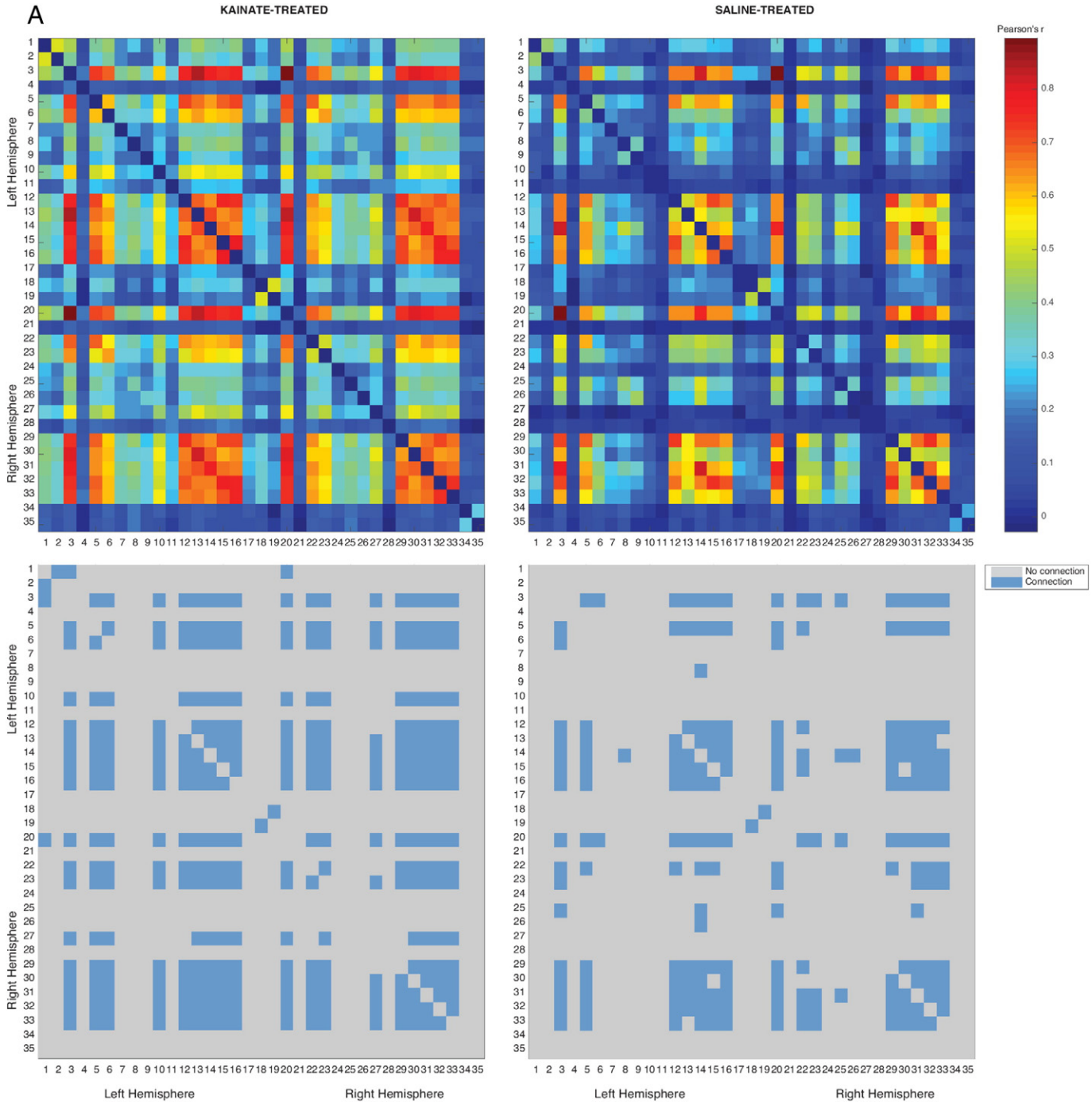

Fig. 1. Correlation matrices derived under 1.5% isoflurane anaesthesia. Top: Correlation matrix consisting of Pearson's correlation coefficients ($-1 < r < 1$) in a network-based statistic framework is shown as a heatmap with significant intra-group connections in the kainate (left, $P \leq 0.001$, $n_{kainate} = 8$) and the control (right, $P \leq 0.007$, $n_{saline} = 7$) group. Bottom: Connectivity matrix shown as a binary heatmap, indicating either connected or disconnected nodes. Refer Table 1 for node labels.

These 78 edges can be classified into connections of several intra- and inter-systems. Most of the increased inter-system connections were between the limbic/subcortical system, the sensorimotor system and the default-mode system, while the intra-system connections were within the structures of the medial temporal lobe.

3.1.2. Differences in connectivity at 2.0% isoflurane

At 2% isoflurane, NBS revealed 218 edges and 33 nodes ($P \leq 0.029$) in the kainate group, compared with 45 edges and 20 nodes ($P \leq 0.136$) in the control group. NBS analysis also revealed a single sub-network comprising of 7 nodes and 6 edges (among a total possible combination of 264 edges) that was significantly higher in the kainate group than the control group (Figure 3B, $P \leq 0.016$). These 6 edges together could not be classified as part of a single system. However, a limbic network involvement was apparent. No nodes and edges corresponded to a reduced connectivity in the kainate group compared to the control group (Fig. 5). A limited number of nodes with higher connectivity in the kainate-treated rats relative to controls were detected in the medial

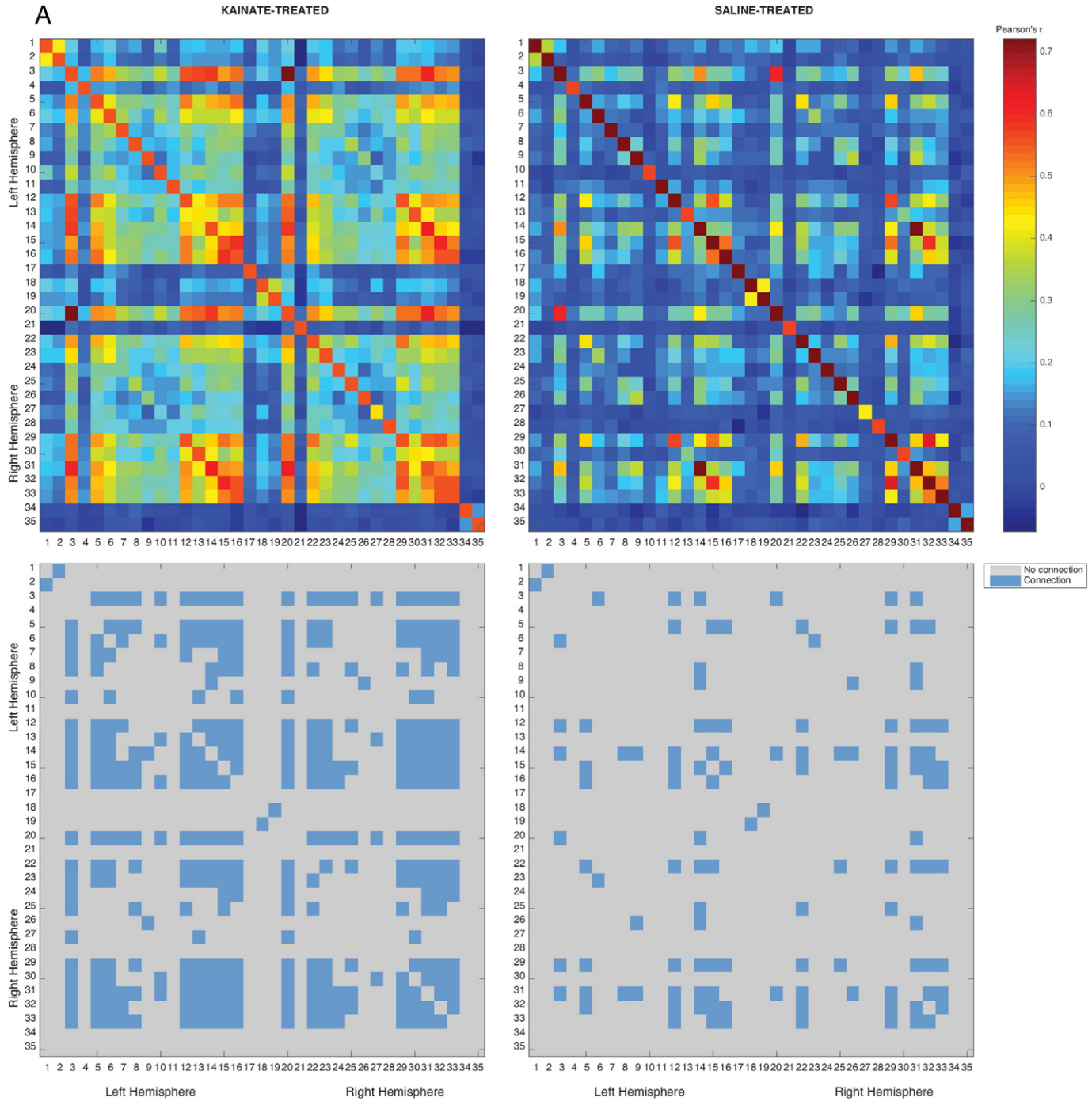

Fig. 2. Correlation matrices derived under 2.0% isoflurane anaesthesia. Top: Correlation matrix consisting of Pearson's correlation coefficients ($-1 < r < 1$) in a Network-based statistic framework is shown as a heatmap with significant intra-group connections in the kainate (left, $P \leq 0.029$, $n_{kainate} = 7$) and the control (right, $P \leq 0.136$ (NS), $n_{saline} = 7$). Bottom: Connectivity matrix shown as a binary heatmap, indicating either connected or disconnected nodes. Refer Table 1 for node labels.

septum, left retrosplenial cortex, right MDT, amygdala bilaterally, and piriform cortex bilaterally (Fig. 5). The specific ROI connections are detailed in Table 1.

3.1.3. Global parameters of the brain functional networks

At 1.5% isoflurane, the global network parameters (C_w, L_w, E_{glob}, E_{loc}) were different between kainate and control groups. Analysis revealed a significantly higher value (all with Bonferroni adjustment) of E_{glob} ($W = 56$, $P \leq 0.0003$), E_{loc} ($W = 53$, $P < 0.002$), and C_w ($W = 55$, $P \leq 0.0006$), but not L_w, in the functional networks of the kainate rats compared with control rats.

At 2.0% isoflurane, the global network parameters (C_w, L_w, E_{glob}, E_{loc}) were also different between kainate and control groups. Analysis revealed a significantly higher value (all with Bonferroni adjustment) of E_{glob} ($W = 49$, $P < 0.0005$), E_{loc} ($W = 49$, $P < 0.0005$), and C_w ($W = 48$, $P < 0.0005$), but not L_w, in the functional networks of the kainate rats compared with control rats (Fig. 6).

3.1.4. Regional parameters of the rat brain functional networks at 1.5% and 2.0% isoflurane

A regional network parameter betweenness centrality (B_i) was different between kainate and control groups. At 1.5% isoflurane, four brain regions exhibited a significant between-group difference in

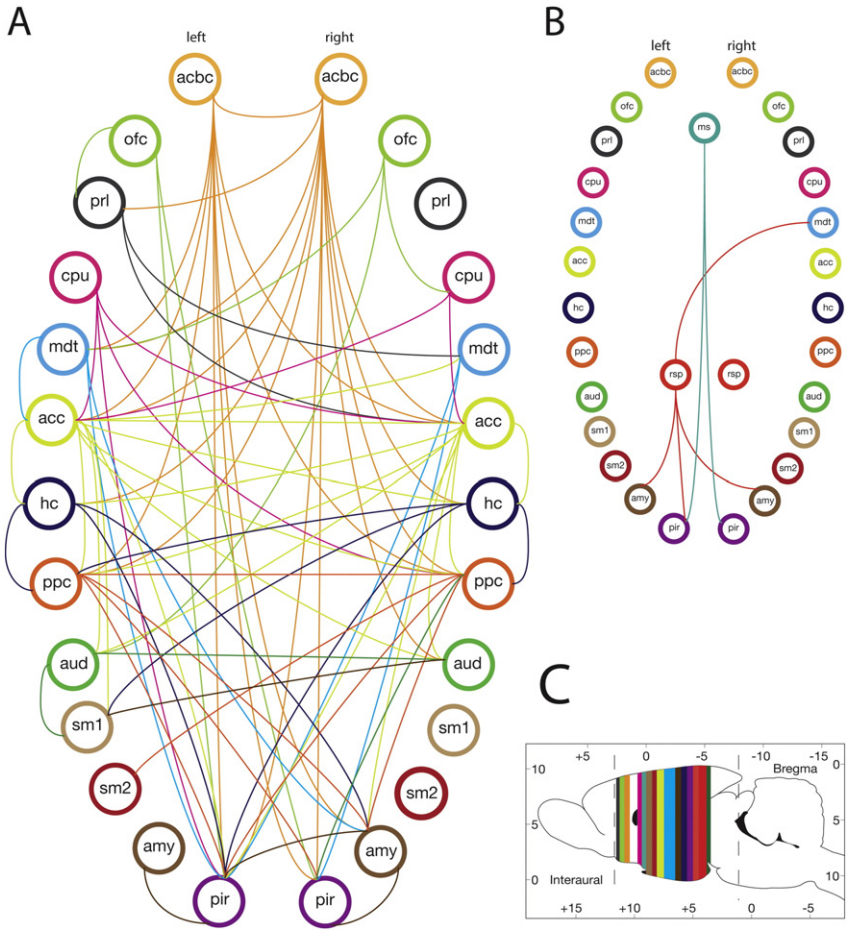

Fig. 3. Connectivity graph shows higher connectivity in kainate-treated than saline-treated group. Connectivity graph for A: Isoflurane 1.5%, B: Isoflurane 2.0%, C: Approximate coronal location for the ROI (color coded). The circles with labels represent brain regions (nodes) and the line represents a significant connection between the two nodes. This sub-network was thresholded at $t \geq 3.5$, with $P < 0.05$. See Table 1 for node abbreviations; left and right pairs of a region are illustrated.

betweenness centrality, including the prelimbic cortex (PrL-LH; $W = 43$, $P < 0.012$), caudate putamen (CPu-LH; $W = 8$, $P < 0.042$), posterior parietal cortex (PPC-LH; $W = 0$, $P < 0.0006$), and auditory/temporal association cortex (Aud-RH; $W = 5$, $P < 0.012$). These same structures also had significantly different B_i at 2.0% isoflurane between kainate-treated and control rats.

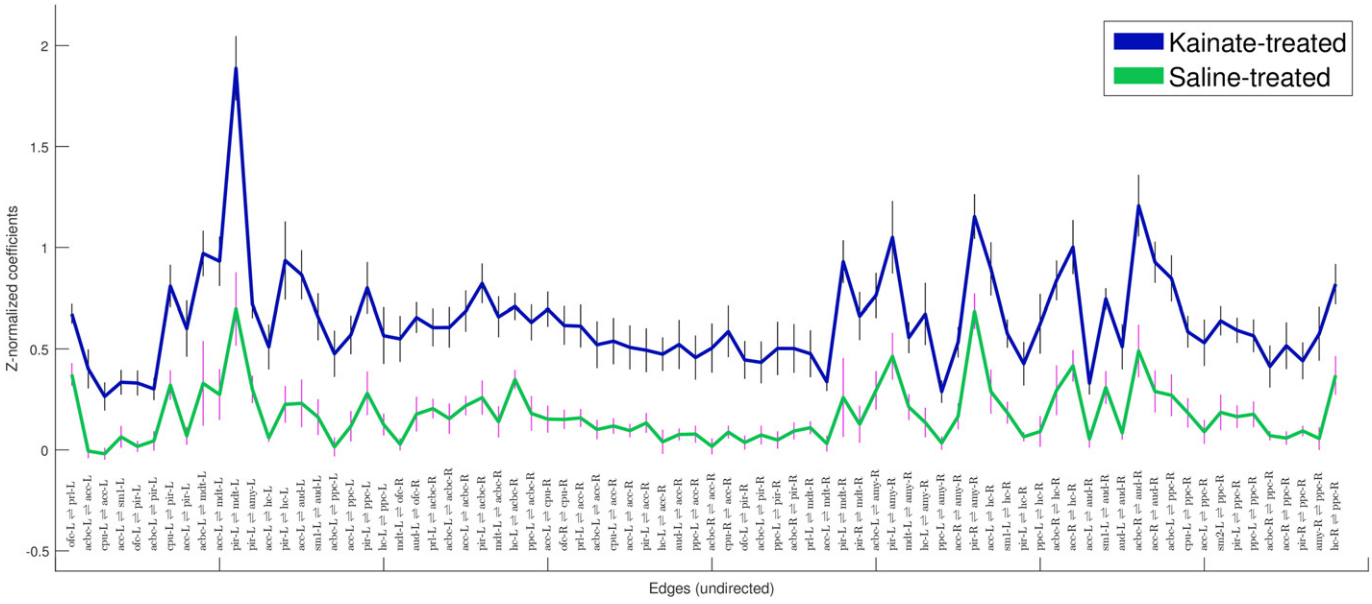

Fig. 4. Mean ± SEM of Fisher's *Z*-correlation coefficients of the edges (undirected connections) that were significantly different between kainate- and saline-treated groups, recorded at 1.5% isoflurane ($P < 0.002$). Edges (each edge defined by a pair of nodes) are labeled on the x-axis. See Table 1 for node abbreviations, and tabulated data in Table 2.

Table 2
Statistically significant undirected edges of the functional networks – kainate-treated group > controls, under 1.5% isoflurane, as shown in Fig. 3A. Source and target nodes do not imply directional connectivity, and edge is non-directional, LH = left hemisphere; RH = right hemisphere.

Source node	Target node	t-stat, $P < 0.002$
Prelimbic cortex - LH	Orbitofrontal cortex - LH	4.26
Anterior cingulate cortex - LH	Nucleus accumbens core - LH	4.53
Anterior cingulate cortex - LH	Caudate putamen - LH	3.87
Primary somatosensory cortex - LH	Anterior cingulate cortex - LH	3.63
Piriform cortex - LH	Orbitofrontal cortex - LH	4.39
Piriform cortex - LH	Nucleus accumbens core - LH	4.82
Piriform cortex - LH	Caudate putamen - LH	4.35
Piriform cortex - LH	Anterior cingulate cortex - LH	5.61
Mediodorsal thalamic nuclei - LH	Nucleus accumbens core - LH	3.78
Mediodorsal thalamic nuclei - LH	Anterior cingulate cortex - LH	4.49
Mediodorsal thalamic nuclei - LH	Piriform cortex - LH	4.53
Amygdala - LH	Piriform cortex - LH	3.87
Hippocampus - LH	Anterior cingulate cortex - LH	4.40
Hippocampus - LH	Piriform cortex - LH	3.86
Auditory/temporal association cortex - LH	Anterior cingulate cortex - LH	3.95
Auditory/temporal association cortex - LH	Primary somatosensory cortex - LH	3.78
Posterior parietal cortex - LH	Nucleus accumbens core - LH	4.34
Posterior parietal cortex - LH	Anterior cingulate cortex - LH	4.87
Posterior parietal cortex - LH	Piriform cortex - LH	4.63
Posterior parietal cortex - LH	Hippocampus - LH	3.83
Orbitofrontal cortex - RH	Mediodorsal thalamic nuclei - LH	5.24
Orbitofrontal cortex - RH	Auditory/temporal association cortex - LH	4.07
Nucleus accumbens core - RH	Prelimbic cortex - LH	3.51
Nucleus accumbens core - RH	Nucleus accumbens core - LH	4.21
Nucleus accumbens core - RH	Anterior cingulate cortex - LH	5.03
Nucleus accumbens core - RH	Piriform cortex - LH	4.97
Nucleus accumbens core - RH	Mediodorsal thalamic nuclei - LH	3.71
Nucleus accumbens core - RH	Hippocampus – LH	3.69
Nucleus accumbens core - RH	Posterior parietal cortex - LH	4.07
Caudate putamen - RH	Anterior cingulate cortex - LH	4.62
Caudate putamen - RH	Orbitofrontal cortex - RH	3.99
Anterior cingulate cortex - RH	Prelimbic cortex - LH	4.78
Anterior cingulate cortex - RH	Nucleus accumbens core - LH	4.53
Anterior cingulate cortex - RH	Caudate putamen - LH	3.87
Anterior cingulate cortex - RH	Anterior cingulate cortex - LH	4.76
Anterior cingulate cortex - RH	Piriform cortex - LH	4.50
Anterior cingulate cortex - RH	Hippocampus - LH	3.77
Anterior cingulate cortex - RH	Auditory/temporal association cortex - LH	3.99
Anterior cingulate cortex - RH	Posterior parietal cortex - LH	4.80
Anterior cingulate cortex - RH	Nucleus accumbens core - RH	4.58
Anterior cingulate cortex - RH	Caudate putamen - RH	4.03
Piriform cortex - RH	Orbitofrontal cortex - LH	3.87
Piriform cortex - RH	Nucleus accumbens core - LH	4.39
Piriform cortex - RH	Posterior parietal cortex - LH	3.52
Piriform cortex - RH	Nucleus accumbens core - RH	3.97
Mediodorsal thalamic nuclei - RH	Prelimbic cortex - LH	3.68
Mediodorsal thalamic nuclei - RH	Anterior cingulate cortex - LH	4.09
Mediodorsal thalamic nuclei - RH	Piriform cortex - LH	3.69
Mediodorsal thalamic nuclei - RH	Piriform cortex - RH	3.60
Amygdala - RH	Nucleus accumbens core - LH	3.72
Amygdala - RH	Piriform cortex - LH	3.66
Amygdala - RH	Mediodorsal thalamic nuclei - LH	3.77
Amygdala - RH	Hippocampus - LH	3.65
Amygdala - RH	Posterior parietal cortex - LH	3.69
Amygdala - RH	Anterior cingulate cortex - RH	3.62
Amygdala - RH	Piriform cortex - RH	4.07
Hippocampus - RH	Anterior cingulate cortex - LH	5.60
Hippocampus - RH	Primary somatosensory cortex - LH	3.90
Hippocampus - RH	Piriform cortex - LH	3.97
Hippocampus - RH	Posterior parietal cortex - LH	3.81
Hippocampus - RH	Nucleus accumbens core - RH	4.21
Hippocampus - RH	Anterior cingulate cortex - RH	4.17
Auditory/temporal association cortex - RH	Anterior cingulate cortex - LH	4.69
Auditory/temporal association cortex - RH	Primary somatosensory cortex - LH	3.98
Auditory/temporal association cortex - RH	Auditory/temporal association cortex - LH	3.57
Auditory/temporal association cortex - RH	Nucleus accumbens core - RH	4.69
Auditory/temporal association cortex - RH	Anterior cingulate cortex - RH	5.37
Posterior parietal cortex - RH	Nucleus accumbens core - LH	3.89
Posterior parietal cortex - RH	Caudate putamen - LH	3.62
Posterior parietal cortex - RH	Anterior cingulate cortex - LH	4.40
Posterior parietal cortex - RH	Primary somatosensory cortex - LH	3.51
Posterior parietal cortex - RH	Piriform cortex - LH	3.67
Posterior parietal cortex - RH	Posterior parietal cortex - LH	3.82
Posterior parietal cortex - RH	Nucleus accumbens core - RH	3.85
Posterior parietal cortex - RH	Anterior cingulate cortex - RH	3.86
Posterior parietal cortex - RH	Piriform Cortex - RH	3.75
Posterior parietal cortex - RH	Amygdala - RH	3.96
Posterior parietal cortex - RH	Hippocampus - RH	3.50

3.1.5. Small-worldness of networks in kainate model of TLE

At 1.5% isoflurane, small-worldness parameter σ was found to be 1.04 ± 0.02 (mean ± SEM) for the kainate group and $\sigma = 1.32 \pm 0.06$ for the control group, indicating that the clustering coefficients γ were on an average approximately 1.26 times higher than those of a comparable random network (equivalent number of vertices, N and edges, K, and same degree distribution) for both subject groups. The small-worldness parameter γ was significantly different between the kainate and control groups ($W = 0$, $P < 0.003$, with Bonferroni adjustment). In addition, we found $\lambda = 0.75 \pm 0.04$ for the kainate group, which was not significantly different from $\lambda = 0.85 \pm 0.14$ for the control group. These λ values approach unity, suggesting that the path lengths for the two groups approximate those of random networks.

At 2.0% isoflurane small-worldness parameter, σ was found to be 1.05 ± 0.01 (mean ± SEM) for the kainate group, not significantly different from $\sigma = 0.92 \pm 0.16$ for the control group ($W = 23$, $P < 0.9$, with Bonferroni adjustment). The clustering coefficients γ were on an average approximately 1.14 times higher than those of a comparable random network for both subject groups. In addition, we found $\lambda = 0.93 \pm 0.02$ for the kainate group, which was not significantly different from $\lambda = 0.96 \pm 0.04$ for the control group.

3.2. Histological assessment

Blind assessment of the histological brain sections showed the highest neuronal damage in CA3c, CA1, and CA3b in the dorsal

Table 3
Statistically significant undirected edges of the functional networks – kainate-treated > controls under 2.0% isoflurane. See Fig. 3B for a graphical representation. Source and target nodes do not imply directional connectivity.

Source node	Target node	t-stat, $P < 0.002$
Piriform cortex - LH	Retrosplenial cortex - LH	3.54
Retrosplenial cortex - LH	Amygdala - LH	4.41
Piriform cortex - LH	Medial septum	4.75
Medial septum	Piriform cortex - RH	3.77
Retrosplenial cortex - LH	Mediodorsal thalamic nuclei - RH	3.70
Retrosplenial cortex - LH	Amygdala - RH	3.83

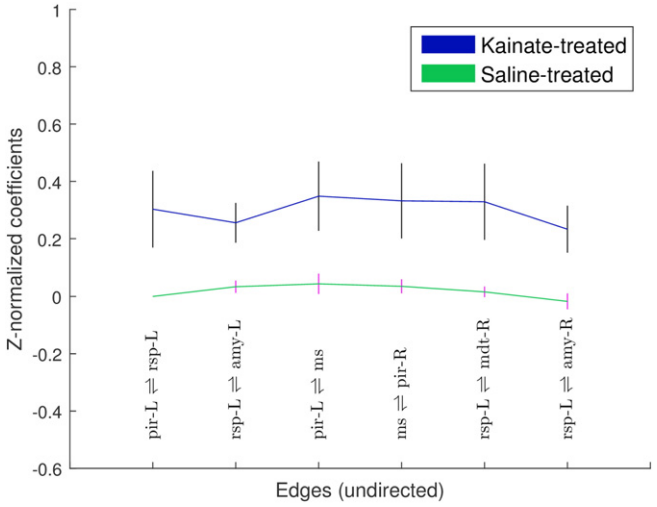

Fig. 5. *Z*-correlation coefficients (mean ± SEM) of edges (undirected connections) that are significantly different between the kainate- and the saline-treated groups, recorded at 2.0% isoflurane ($P < 0.016$). Edges (each edge defined by a pair of nodes) are labeled on the x-axis, and tabulated sequentially in Table 3. See Table 1 for node abbreviations.

hippocampus, with little damage in CA2 and subiculum. In extrahippocampal structures, the MDT, followed by medial septum and piriform cortex, showed the most frequent damage, while clear alterations were not observed in the anterior and posterior cingulate cortex, infralimbic cortex, caudate-putamen or nucleus accumbens. Lateral and third ventricle expansions were apparent in the kainate-treated as compared to control rats, often accompanied by severe damage in the MDT and medial septum. The histological damage was not uniform, but all kainate-treated rats showed observable neuronal damage in the brain (typically in CA3c, see Supplementary Fig. S1), while none of the saline-treated rats showed any detectable damage in the brain.

4. Discussion

In this study, we showed that the interictal resting state networks in the brain, during 1.5% and 2% isoflurane anaesthesia, were altered following a kainic acid induced status epilepticus model of TLE. Graph theoretical analysis reveals enhanced functional connectivity among limbic and DMN structures in kainate-treated rats compared to saline-treated controls. The main findings are: a) increased clustering of the whole brain networks, notably the DMN and the temporal lobe networks, b) both inter- and intra-hemispheric connectivity increased in the epileptic brain, c) the small-worldness parameter, σ, was significantly lower in epileptic animals.

4.1. Differences in functional connectivity between epileptic and control brains

In the present study, kainate-treated rats as compared to control rats showed structures with significant connections, in descending order of the number of edges–anterior cingulate cortex (edges = 31), nucleus accumbens core (21), piriform cortex (21), hippocampus (13), auditory/temporal association cortex (10), MDT (10), amygdala (9), caudate putamen (7) and orbitofrontal cortex (6). While this list would be affected by the ROIs selected, the present list indicates increases in functional connectivity in a limbic network and DMN.

4.1.1. Increased connectivity within a limbic network

The limbic network that showed increased connectivity in kainate-treated as compared to control rats appear to be similar to that activated by severe limbic seizures. [^{14}C]2-deoxyglucose autoradiography showed that generalized convulsive seizures involved bilaterally the hippocampal formation, amygdala, nucleus accumbens, substantia nigra (Collins et al., 1983), ventral pallidum, globus pallidus, MDT and frontal motor cortex (Clifford et al., 1987). In this study, we confirmed histologically the neuronal damage in the MDT, piriform cortex, and medial septal region, in addition to that in the hippocampus, reported previously after kainate-induced SE (Chen and Buckmaster, 2005). MDT, which has connections with the cingulate cortex (Delevich et al.,

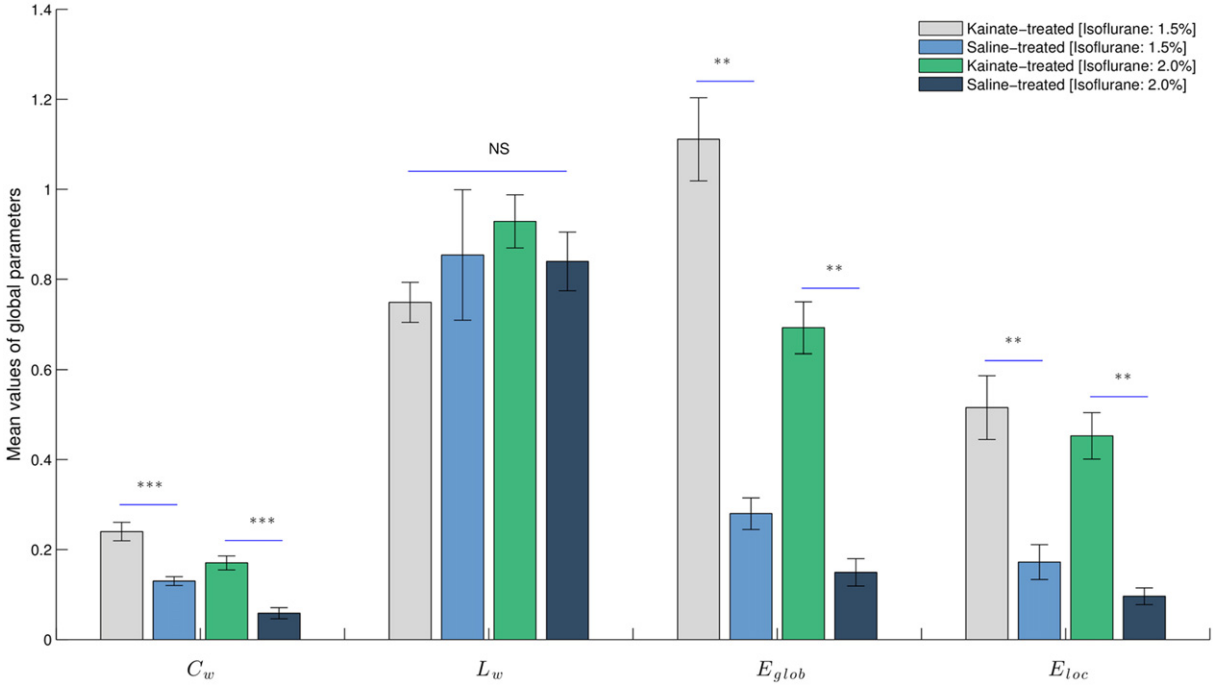

Fig. 6. Global parameters are different between kainate-treated and saline-treated groups. Statistical comparison of the global parameters (C_w, L_w, E_{glob}, E_{loc}) of the functional networks in the kainate-treated and saline-treated groups at 1.5% and 2.0% isoflurane concentrations. Results are expressed as mean ± SEM. ** signifies $P < 0.002$, *** signifies $P < 0.0001$ and NS – not statistically significant.

2015), was inferred to be involved in generalized motor seizures (Cassidy and Gale, 1998; Patel et al., 1988). A similar network has been described in human TLE (Spencer, 2002). Increased functional connectivity between limbic and other structures may result from mechanisms induced by repeated or prolonged seizures – axonal sprouting, loss of inhibition, increase in excitation (long-term potentiation) and increase in spike excitability. After SE, axon sprouting of granule cells would increase recurrent excitation in the dentate gyrus (Tauck and Nadler, 1985), whereas axonal sprouting of CA1 pyramidal cell would increase CA1 to subiculum excitation (Cavazos et al., 2004). Anatomical projections from the basolateral amygdala to ventral subiculum were also increased after pilocarpine SE (Ma et al., 2015). In the hippocampus, kainate-induced SE resulted in loss of inhibitory interneurons in the distal dendritic layer (Cossart et al., 2001), increase in dendritic excitation and spike excitability (Bernard et al., 2004; Wu and Leung, 2003). Canals et al. (2009) reported increased BOLD signal in the prefrontal cortex and nucleus accumbens, and in hippocampal-entorhinal cortex connectivity bilaterally following LTP induced by perforant path stimulation. Similarly, multisynaptic excitatory pathways in the hippocampus-entorhinal cortex neural circuit were increased after kainate-SE and kindled seizures (Leung, 2009; Wu and Leung, 2003). The piriform cortex, which showed decreased GABAergic neurons after SE (Freichel et al., 2006), may have a significant role to play in enhancing functional connectivity in epileptic rats. The piriform cortex has been identified as an important node initiating generalized seizures in rats (Cassidy and Gale, 1998), and mediating the propagation of interictal discharges in focal epilepsies in humans (Vaughan and Jackson, 2014). Ullal et al. (2005) showed a long-lasting upregulation of GluR5 mRNA and protein after kainate-SE, which may decrease GABA-mediated inhibition (Vincent and Mulle, 2009) and increase functional connectivity.

4.1.2. Increased activity within the DMN

We found increased connectivity within the components of the DMN, including the anterior and posterior cingulate cortex, auditory/temporal association cortex, and the hippocampus, in kainate-treated rats relative to controls. Bilateral components of the DMN, including the anterior cingulate cortex, posterior parietal cortex, and auditory/temporal association cortex were significantly more functionally connected in the epileptic rats as compared to controls. Thalamocortical (MDT and DMN) connectivity was also found to be upregulated. The functional reorganization following SE is likely an expansion of the direct/indirect and multisynaptic projections with the areas that manifested seizure activity, which include temporal lobe structures, MDT and frontal cortex (discussed above). Our results indicate that MDT and anterior cingulate cortex were prominent nodes in a hippocampal-prefrontal and limbic-DMN network in epileptic animals, which is supported by neuroanatomical studies (Vertes, 2006) and fMRI studies in normal rats (Gozzi and Schwarz, 2016; Liang et al., 2013).

The high connectivity within and outside of the DMN in epileptic animals appears to be different from human TLE. In TLE patients (during the interictal state) as compared to control subjects, with a few exceptions (Chiang et al., 2014b), the functional connections within the DMN, and between the DMN and the medial temporal lobe were generally reported to be decreased (James et al., 2013; Kucukboyaci et al., 2013; Liao et al., 2010; Liao et al., 2011; Pittau et al., 2012).

4.1.3. Functional connectivity of the nucleus accumbens

Our results indicated an increase in functional connectivity between nucleus accumbens (NAC) and several limbic and frontal areas in KA-treated rats compared to controls, including the hippocampus, amygdala, piriform cortex, prefrontal cortex, cingulate cortex and MDT. The NAC has been suggested as an interface between the limbic and motor systems, which converts motivation into action (Mogenson et al., 1993). The increased limbic and prefrontal connectivity to the NAC may facilitate an increase in dopaminergic function in the NAC following kainate-induced SE (Ando et al., 2004). Similar hyperdopaminergic functions may follow kindled seizures in the amygdala and hippocampus (Adamec, 1991; Leung et al., 2000). The increased NAC connectivity suggests an increased driving of the NAC by the afferent pathways from the hippocampus, amygdala, prefrontal and other cortices (Groenewegen et al., 1987; Groenewegen and Trimble, 2007). Increased functional connectivity of the basal ganglia with the amygdala may underlie the emotional and affective alterations in TLE animal models (Adamec, 1990). Contrary to our findings, reduced functional connectivity between the hippocampus or amygdala with the nucleus accumbens and ventromesial limbic prefrontal cortex has been reported in TLE patients (Pittau et al., 2012).

4.1.4. Alterations in graph metrics

The graph topological properties measuring integration and segregation were significantly altered in epileptic rats compared to controls. We found a significantly higher clustering coefficient (C_w), global efficiency (E_{glob}), and local efficiency (E_{loc}) in epileptic rats compared to controls. The path length was short and similar between epileptic and control rats. A high C_w implies relatively high local connectedness of brain regions, as was found for the limbic and DMN structures. Short absolute path lengths are suggested to promote effective interactions and processing among connected regions. Increased local efficiency can be attributed to the increased connectivity within the limbic network. In a computational study investigating DG epileptogenesis, Dyhrfjeld-Johnsen et al. (2007) found altered local and long range connections, in support of the present results of increased clustering coefficient, global efficiency, and small-world findings for local computations.

In TLE patients compared to controls, the clustering coefficient estimates from fMRI functional connectivity were shown to be decreased (Liao et al., 2010) or not significantly changed (Chiang and Haneef, 2014a). Structural and physiological (EEG/EMG) estimates of the clustering coefficient also showed either an increase (Bernhardt et al., 2011; Bonilha et al., 2012; Horstmann et al., 2010) or a decrease (Vaessen et al., 2012) in TLE patients compared to control subjects.

4.2. Network-level anaesthetic effects

The functional network architecture of the brain has been shown to be preserved at low levels of anaesthesia in rodents (Wang et al., 2011) and non-human primates (Hutchison et al., 2014). In the kainate model, the number of nodes and connectivity found at 1.5 % v/v isoflurane was greatly diminished at 2.0 % v/v isoflurane, although some network architecture persisted. Interestingly, a few nodes (at the medial septum, and retrosplenial cortex) were present at 2% but not 1.5% isoflurane. Other nodes at the piriform cortex, MDT and basolateral amygdala persisted at both levels of anaesthesia. Multiple brain areas in the limbic system, including the medial septum and hippocampus, are known to affect sensitivity to general anaesthesia (Leung et al., 2014; Ma et al., 2002). Kainate-treated as compared to control rats showed a higher isoflurane sensitivity to loss of righting (Gill & Leung, unpublished data). However, a higher behavioural sensitivity to isoflurane in kainate-treated than control rats would suggest a greater hypnotic effect at a fixed isoflurane dose, which may predict a general decrease in functional connectivity (Hutchison et al., 2014; Liang et al., 2011) in kainate-treated than control rats. Thus, the present results of an increase in functional connectivity in kainate-treated as compared to control rats are not readily explained by difference in isoflurane sensitivity.

4.3. Disparity with human literature

Our fMRI results of the kainate-induced SE model both support and apparently contradict the human literature. Disparity between an animal TLE model and the human condition may result from a number of reasons. In TLE patients, the seizure focus is commonly unilateral, starting in the hippocampus, amygdala, entorhinal or perirhinal cortex. KA-induced seizures involve the hippocampus bilaterally (Ben-Ari,

1985; Lévesque and Avoli, 2013). Results from human TLE may be confounded by a number of factors that include cerebral functional reserve, age, gender, antiepileptic drugs, etiology and duration of epilepsy. Human TLE does not typically arise from status epilepticus. The detailed histopathology of TLE (Blümcke et al., 2013) may differ from that of kainate rats.

Similar to the TLE animal model, the cortical BOLD response in animal models of generalized spike-wave discharges has consistently failed to show the decrease reported in human generalized seizures (Youngblood et al., 2015). A difference between animal and human BOLD response in epilepsy was suggested to arise from the use of general anaesthesia in animals, as compared to no anaesthesia in humans during fMRI (Youngblood et al., 2015). However, this suggestion remains to be tested.

4.4. Caveats and limitations

Firstly, the coarse resolution of $800 \times 800\ \mu m^2$ ($400 \times 400\ \mu m^2$ before spatial smoothing) with 1 mm slice thickness considerably limits our ability to differentiate between small yet distinct brain structures that are close together. Secondly, no causality or effective connectivity could be determined since we used undirected networks. Third, although the resting state networks were found in rodents under anaesthesia, an effect of isoflurane on the networks could not be excluded. Fourth, we pre-selected the seed regions in each of the rats, while an ICA-optimized approach may recognize spatiotemporal activation without selection bias. Lastly, a volumetric gradient coil, not available during the present study, may improve contrast-to-noise ratio of the BOLD signal from ventral brain structures.

4.5. Conclusions

In conclusion, in the kainate model of TLE, we found an increase in functional connectivity within the medial temporal regions and the limbic network, and the anterior and posterior DMN shared a better connection. Furthermore, as compared to control, the kainate TLE model showed an increased clustering coefficient, shorter path length and higher level of global and local efficiency along with altered small-world topology.

This study supports the notion that TLE is a network disorder, rather than a disorder of a small part of the brain, such as the seizure focus in the temporal lobe. The aberrant networks may help to explain the behavioural, cognitive, psychiatric and neurological symptoms related to TLE, and restoration of normal networks can be a target of therapeutic treatment.

Acknowledgements

We would like to thank Dr. Matthew Hutchison and Dr. Ravi Menon for the invaluable discussions; and Ashley Kirley, Alex Li, and Miranda Bellyou for technical assistance. This research was financially supported by operating grants from the Natural Sciences and Engineering Research Council of Canada grant 1037-2013, Canadian Institutes of Health Research grant MOP-15685, and EpLink, the Epilepsy Research Program of Ontario Brain Institute.

Appendix A. Supplementary data

Supplementary data to this article can be found online at http://dx.doi.org/10.1016/j.nicl.2016.11.002.

References

Adamec, R.E., 1990. Does kindling model anything clinically relevant? Biol. Psychiatry 27 (3), 249–279.
Adamec, R.E., 1991. Partial kindling of the ventral hippocampus: identification of changes in limbic physiology which accompany changes in feline aggression and defense. Physiol. Behav. 49 (3), 443–453.
Ando, N., Morimoto, K., Watanabe, T., Ninomiya, T., Suwaki, H., 2004. Enhancement of central dopaminergic activity in the kainate model of temporal lobe epilepsy: implication for the mechanism of epileptic psychosis. Neuropsychopharmacology 29 (7), 1251–1258.
Bartolomei, F., Wendling, F., Régis, J., Gavaret, M., Guye, M., Chauvel, P., 2004. Pre-ictal synchronicity in limbic networks of mesial temporal lobe epilepsy. Epilepsy Res. 61 (1–3), 89–104.
Bastian, M., Heymann, S., Jacomy, M., 2009. Gephi: an open source software for exploring and manipulating networks. Third International AAAI Conference on Weblogs and Social Media, pp. 361–362.
Ben-Ari, Y., 1985. Limbic seizure and brain damage produced by kainic acid: mechanisms and relevance to human temporal lobe epilepsy. Neuroscience 14 (2), 375–403.
Bernard, C., Anderson, A., Becker, A., Poolos, N.P., Beck, H., Johnston, D., 2004. Acquired dendritic channelopathy in temporal lobe epilepsy. Science 305 (5683), 532–535.
Bernhardt, B.C., Chen, Z., He, Y., Evans, A.C., Bernasconi, N., 2011. Graph-theoretical analysis reveals disrupted small-world organization of cortical thickness correlation networks in temporal lobe epilepsy. Cereb. Cortex 21 (9), 2147–2157.
Bernhardt, B.C., Bonilha, L., Gross, D.W., 2015. Network analysis for a network disorder: the emerging role of graph theory in the study of epilepsy. Epilepsy Behav. 50, 162–170.
Bertram, E.H., Zhang, D.X., Mangan, P., Fountain, N., Rempe, D., 1998. Functional anatomy of limbic epilepsy: a proposal for central synchronization of a diffusely hyperexcitable network. Epilepsy Res. 32 (1–2), 194–205.
Blümcke, I., Thom, M., Aronica, E., Armstrong, D.D., Bartolomei, F., Bernasconi, A., Bernasconi, N., Bien, C.G., Cendes, F., Coras, R., Cross, J.H., 2013. International consensus classification of hippocampal sclerosis in temporal lobe epilepsy: a task force report from the ILAE commission on diagnostic methods. Epilepsia 54, 1315–1329.
Bonilha, L., Nesland, T., Martz, G.U., Joseph, J.E., Spampinato, M.V., Edwards, J.C., Tabesh, A., 2012. Medial temporal lobe epilepsy is associated with neuronal fibre loss and paradoxical increase in structural connectivity of limbic structures. J. Neurol. Neurosurg. Psychiatry 83 (9), 903–909.
Buckmaster, P.S., 2004. Laboratory animal models of temporal lobe epilepsy. Comp. Med. 54 (5), 473–485.
Bullmore, E., Sporns, O., 2009. Complex brain networks: graph theoretical analysis of structural and functional systems. Nature reviews. Nat. Rev. Neurosci. 10 (3), 186–198.
Canals, S., Beyerlein, M., Merkle, H., Logothetis, N.K., 2009. Functional MRI evidence for LTP-induced neural network reorganization. Curr. Biol. 19, 398–403.
Cassidy, R.M., Gale, K., 1998. Mediodorsal thalamus plays a critical role in the development of limbic motor seizures. J. Neurosci. 18 (21), 9002–9009.
Cavazos, J.E., Jones, S.M., Cross, D.J., 2004. Sprouting and synaptic reorganization in the subiculum and CA1 region of the hippocampus in acute and chronic models of partial-onset epilepsy. Neuroscience 126 (3), 677–688.
Chen, S., Buckmaster, P.S., 2005. Stereological analysis of forebrain regions in kainate-treated epileptic rats. Brain Res. 1057 (1–2), 141–152.
Chiang, S., Haneef, Z., 2014a. Graph theory findings in the pathophysiology of temporal lobe epilepsy. Clin. Neurophysiol. 125 (7), 1295–1305.
Chiang, S., Stern, J.M., Engel, J., Levin, H.S., Haneef, Z., 2014b. Differences in graph theory functional connectivity in left and right temporal lobe epilepsy. Epilepsy Res. 108 (10), 1770–1781.
Clifford, D.B., Olney, J.W., Maniotis, A., Collins, R.C., Zorumski, C.F., 1987. The functional anatomy and pathology of lithium-pilocarpine and high-dose pilocarpine seizures. Neuroscience 23 (3), 953–968.
Collins, R.C., Tearse, R.G., Lothman, E.W., 1983. Functional anatomy of limbic seizures: focal discharges from medial entorhinal cortex in rat. Brain Res. 280 (1), 25–40.
Cossart, R., Dinocourt, C., Hirsch, J.C., Merchan-Perez, A., De Felipe, J., Ben-Ari, Y., Esclapez, M., Bernard, C., 2001. Dendritic but not somatic GABAergic inhibition is decreased in experimental epilepsy. Nat. Neurosci. 4 (1), 52–62.
Cox, R.W., 1996. AFNI: software for analysis and visualization of functional magnetic resonance neuroimages. Comput. Biomed. Res. 29 (3), 162–173.
Delevich, K., Tucciarone, J., Huang, Z.J., Li, B., 2015. The mediodorsal thalamus drives feedforward inhibition in the anterior cingulate cortex via parvalbumin interneurons. J. Neurosci. 35 (14), 5743–5753.
Dudek, J.L.H., Edward, F., 2005. Chemoconvulsant model of chronic spontaneous seizures - kainic acid protocol. Curr. Protoc. Neurosci. 1–12 (Supplement).
Dyhrfjeld-Johnsen, J., Santhakumar, V., Morgan, R.J., Huerta, R., Tsimring, L., Soltesz, I., 2007. Topological determinants of epileptogenesis in large-scale structural and functional models of the dentate gyrus derived from experimental data. J. Neurophysiol. 97 (2), 1566–1587.
Freichel, C., Potschka, H., Ebert, U., Brandt, C., Löscher, W., 2006. Acute changes in the neuronal expression of GABA and glutamate decarboxylase isoforms in the rat piriform cortex following status epilepticus. Neuroscience 141 (4), 2177–2194.
Gozzi, A., Schwarz, A.J., 2016. Large-scale functional connectivity networks in the rodent brain. NeuroImage 127, 496–509.
Greicius, M.D., Supekar, K., Menon, V., Dougherty, R.F., 2009. Resting-state functional connectivity reflects structural connectivity in the default mode network. Cereb. Cortex 19 (1), 72–78.
Groenewegen, H.J., Trimble, M., 2007. The ventral striatum as an interface between the limbic and motor systems. CNS Spectr. 12, 887–892.
Groenewegen, H.J., Vermeulen-Van der Zee, E., Te Kortschot, A., Witter, M.P., 1987. Organization of the projections from the subiculum to the ventral striatum in the rat. A study using anterograde transport of *Phaseolus vulgaris* leucoagglutinin. Neuroscience 23 (1), 103–120.

Hampson, M., Peterson, B.S., Skudlarski, P., Gatenby, J.C., Gore, J.C., 2002. Detection of functional connectivity using temporal correlations in MR images. Hum. Brain Mapp. 15, 247–262.
Horstmann, M.T., Bialonski, S., Noennig, N., Mai, H., Prusseit, J., Wellmer, J., Hinrichs, H., Lehnertz, K., 2010. State dependent properties of epileptic brain networks: comparative graph-theoretical analyses of simultaneously recorded EEG and MEG. Clin. Neurophysiol. 121 (2), 172–185.
Hutchison, R.M., Mirsattari, S.M., Jones, C.K., Gati, J.S., Leung, L.S., 2010. Functional networks in the anesthetized rat brain revealed by independent component analysis of resting-state FMRI. J. Neurophysiol. 103 (6), 3398–3406.
Hutchison, R.M., Hutchison, M., Manning, K.Y., Menon, R.S., Everling, S., 2014. Isoflurane induces dose-dependent alterations in the cortical connectivity profiles and dynamic properties of the brain's functional architecture. Hum. Brain Mapp. 35 (12), 5754–5775.
James, G.A., Tripathi, S.P., Ojemann, J.G., Gross, R.E., Drane, D.L., 2013. Diminished default mode network recruitment of the hippocampus and parahippocampus in temporal lobe epilepsy. J. Neurosurg. 119 (2), 288–300.
Jenkinson, M., Beckmann, C.F., Behrens, T.E.J., Woolrich, M.W., Smith, S.M., 2012. FSL. NeuroImage 62 (2), 782–790.
Klassen, L.M., Menon, R.S., 2004. Robust automated shimming technique using arbitrary mapping acquisition parameters (RASTAMAP). Magn. Reson. Med. 51, 881–887.
Kucukboyaci, N.E., Kemmotsu, N., Cheng, C.E., Girard, H.M., Tecoma, E.S., Iragui, V.J., McDonald, C.R., 2013. Functional connectivity of the hippocampus in temporal lobe epilepsy: feasibility of a task-regressed seed-based approach. Brain Connect. 3 (5), 464–474.
Laufs, H., 2012. Functional imaging of seizures and epilepsy: evolution from zones to networks. Curr. Opin. Neurol. 25 (2), 194–200.
Laufs, H., Hamandi, K., Salek-Haddadi, A., Kleinschmidt, A.K., Duncan, J.S., Lemieux, L., 2007. Temporal lobe interictal epileptic discharges affect cerebral activity in "default mode" brain regions. Hum. Brain Mapp. 28, 1023–1032.
Leung, L.S., 2009. Synaptic potentiation and inhibition after partial seizures. In: Schwartzkroin, P.A. (Ed.), Encyclopedia of Basic Epilepsy Research 3. Elsevier: Academic Press, pp. 1204–1210.
Leung, L.S., Ma, J., McLachlan, R.S., 2000. Behaviors induced or disrupted by complex partial seizures. Neurosci. Biobehav. Rev. 24 (7), 763–775.
Leung, L.S., Ma, J., Shen, B., Nachim, I., Luo, T., 2013. Medial septal lesion enhances general anesthesia response. Exp. Neurol. 247, 419–428.
Leung, L.S., Luo, T., Ma, J., Herrick, I., 2014. Brain areas that influence general anesthesia. Prog. Neurobiol. 84, 450–455.
Lévesque, M., Avoli, M., 2013. The kainic acid model of temporal lobe epilepsy. Neurosci. Biobehav. Rev. 37 (10 Pt 2), 2887–2899.
Liang, Z., King, J., Zhang, N., 2011. Uncovering intrinsic connectional architecture of functional networks in awake rat brain. J. Neurosci. 31 (10), 3776–3783.
Liang, Z., Li, T., King, J., Zhang, N., 2013. Mapping thalamocortical networks in rat brain using resting-state functional connectivity. NeuroImage 83, 237–244.
Liao, W., Zhang, Z., Pan, Z., Mantini, D., Ding, J., Duan, X., Luo, C., Lu, G., Chen, H., 2010. Altered functional connectivity and small-world in mesial temporal lobe epilepsy. PLoS ONE 5 (1), e8525.
Liao, W., Zhang, Z., Pan, Z., Mantini, D., Ding, J., Duan, X., Luo, C., Wang, Z., Tan, Q., Lu, G., Chen, H., 2011. Default mode network abnormalities in mesial temporal lobe epilepsy: a study combining fMRI and DTI. Hum. Brain Mapp. 32 (6), 883–895.
Lopes da Silva, F.H., Gorter, J.A., Wadman, W.J., 2012. Epilepsy as a dynamic disease of neuronal networks. Handb. Clin. Neurol. 107, 35–62.
Lu, H., Zou, Q., Gu, H., Raichle, M.E., Stein, E.A., Yang, Y., 2012. Rat brains also have a default mode network. Proc. Natl. Acad. Sci. U. S. A. 109 (10), 3979–3984.
Ma, J., Shen, B., Stewart, L.S., Herrick, I.A., Leung, L.S., 2002. The septohippocampal system participates in general anesthesia. J. Neurosci. 22 (2), RC200.
Ma, D.L., Qu, J.Q., Goh, E.L.K., Tang, F.-R., 2015. Reorganization of basolateral amygdala-subiculum circuitry in mouse epilepsy model. Front. Neuroanat. 9, 167.
Meador, K.J., 2011. Networks, cognition, and epilepsy. Neurology 77 (10), 930–931.
Mirsattari, S.M., Ives, J.R., Bihari, F., Leung, L.S., Menon, R.S., Bartha, R., 2005. Real-time display of artifact-free electroencephalography during functional magnetic resonance imaging and magnetic resonance spectroscopy in an animal model of epilepsy. Magn. Reson. Med. 53 (2), 456–464.
Mogenson, G.J., Brudzynski, S.M., Wu, M., Yang, C.R., Yim, C.C.Y., 1993. From motivation to action: a review of dopaminergic regulation of limbic-nucleus accumbens-ventral pallidum-pedunculopontine nucleus circuitries involved in limbic-motor integration. In: Kalivas P.W, Barnes, C.D. (Eds.), Limbic Motor Circuits and Neuropsychiatry. CRC Press, Boca Raton, pp. 193–225.
Morgan, V.L., Rogers, B.P., Sonmezturk, H.H., Gore, J.C., Abou-Khalil, B., 2011. Cross hippocampal influence in mesial temporal lobe epilepsy measured with high temporal resolution functional magnetic resonance imaging. Epilepsia 52 (9), 1741–1749.
Otte, W.M., Dijkhuizen, R.M., van Meer, M.P., van der Hel, W.S., Verlinde, S.A., van Nieuwenhuizen, O., Viergever, M.A., Stam, C.J., Braun, K.P., 2012. Characterization of functional and structural integrity in experimental focal epilepsy: reduced network efficiency coincides with white matter changes. PLoS ONE 7 (7), e39078.
Patel, S., Millan, M.H., Meldrum, B.S., 1988. Decrease in excitatory transmission within the lateral habenula and the mediodorsal thalamus protects against limbic seizures in rats. Exp. Neurol. 101 (1), 63–74.
Paxinos, G., Watson, C., 2007. The Rat Brain in Stereotaxic Coordinates. sixth ed. 170. Elsevier Academic Press, pp. 547–612.
Pittau, F., Grova, C., Moeller, F., Dubeau, F., Gotman, J., 2012. Patterns of altered functional connectivity in mesial temporal lobe epilepsy. Epilepsia 53 (6), 1013–1023.
Racine, R.J., 1972. Modification of seizure activity by electrical stimulation. II. Motor seizure. Electroencephalogr. Clin. Neurophysiol. 32 (3), 281–294.
Rubinov, M., Sporns, O., 2010. Complex network measures of brain connectivity: uses and interpretations. NeuroImage 52 (3), 1059–1069.
Sierakowiak, A., Monnot, C., Aski, S.N., Uppman, M., Li, T.-Q., Damberg, P., Brené, S., 2015. Default mode network, motor network, dorsal and ventral basal ganglia networks in the rat brain: comparison to human networks using resting state-fMRI. PLoS ONE 10 (3), e0120345.
Spencer, S.S., 2002. Neural networks in human epilepsy: evidence of and implications for treatment. Epilepsia 43 (3), 219–227.
Sperk, G., Lassmann, H., Baran, H., Seitelberger, F., Hornykiewicz, O., 1985. Kainic acid-induced seizures: dose-relationship of behavioural, neurochemical and histopathological changes. Brain Res. 338, 289–295.
Stam, C.J., Reijneveld, J.C., 2007b. Graph theoretical analysis of complex networks in the brain. Nonlinear Biomed. Phys. 1 (1), 3.
Stam, C.J., Jones, B.F., Nolte, G., Breakspear, M., Scheltens, P., 2007a. Small-world networks and functional connectivity in Alzheimer's disease. Cereb. Cortex 17 (1), 92–99.
Tauck, D.L., Nadler, J.V., 1985. Evidence of functional mossy fiber sprouting in hippocampal formation of kainic acid-treated rats. J. Neurosci. 5 (4), 1016–1022.
Tracy, J.I., Osipowicz, K., Spechler, P., Sharan, A., Skidmore, C., Doucet, G., Sperling, M.R., 2014. Functional connectivity evidence of cortico-cortico inhibition in temporal lobe epilepsy. Hum. Brain Mapp. 35 (1), 353–366.
Ullal, G., Fahnestock, M., Racine, R., 2005. Time-dependent effect of kainate-induced seizures on glutamate receptor GluR5, GluR6, and GluR7 mRNA and protein expression in rat hippocampus. Epilepsia 46 (5), 616–623.
Vaessen, M.J., Jansen, J.F.A., Vlooswijk, M.C.G., Hofman, P.A.M., Majoie, H.J.M., Aldenkamp, A.P., Backes, W.H., 2012. White matter network abnormalities are associated with cognitive decline in chronic epilepsy. Cereb. Cortex 22 (9), 2139–2147.
Vaughan, D.N., Jackson, G.D., 2014. The piriform cortex and human focal epilepsy. Front. Neurol. 5, 259.
Vertes, R.P., 2006. Interactions among the medial prefrontal cortex, hippocampus and midline thalamus in emotional and cognitive processing in the rat. Neuroscience 142 (1), 1–20.
Vincent, P., Mulle, C., 2009. Kainate receptors in epilepsy and excitotoxicity. Neuroscience 158 (1), 309–323.
Wang, K., van Meer, M., van der Marel, K., van der Toorn, A., Xu, L., Liu, Y., Viergever, M.A., Jiang, T., Dijkhuizen, R.M., 2011. Temporal scaling properties and spatial synchronization of spontaneous blood oxygenation level-dependent (BOLD) signal fluctuations in rat sensorimotor network at different levels of isoflurane anesthesia. NMR Biomed. 24 (1), 61–67.
Wang, B., Fan, Y., Lu, M., Li, S., Song, Z., Peng, X., Zhang, R., Lin, Q., He, Y., Wang, J., Huang, R., 2013a. Brain anatomical networks in world class gymnasts: a DTI tractography study. NeuroImage 65, 476–487.
Wang, J., Zuo, X., Dai, Z., Xia, M., Zhao, Z., Zhao, X., Jia, J., Han, Y., He, Y., 2013b. Disrupted functional brain connectome in individuals at risk for Alzheimer's disease. Biol. Psychiatry 73 (5), 472–481.
Watts, D.J., Strogatz, S.H., 1998. Collective dynamics of 'small-world' networks. Nature 393, 440–442.
Wu, K., Leung, L.S., 2003. Increased dendritic excitability in hippocampal CA1 in vivo in the kainic acid model of temporal lobe epilepsy: a study using current source density analysis. Neuroscience 116 (2), 599–616.
Youngblood, M.W., Chen, W.C., Mishra, A.M., Enamandram, S., Sanganahalli, B.G., Motelow, J.E., Bai, H.X., Frohlich, F., Gribizis, A., Lighten, A., Hyder, F., 2015. Rhythmic 3–4 Hz discharge is insufficient to produce cortical BOLD fMRI decreases in generalized seizures. NeuroImage 109, 368–377.
Zalesky, A., Fornito, A., Bullmore, E.T., 2010. Network-based statistic: identifying differences in brain networks. NeuroImage 53, 1197–1207.